Review

John N. Sherwood: Studies of Energetic Materials

Published as part of a Crystal Growth and Design virtual special issue Celebrating John N. Sherwood, Pioneer in Organic and Molecular Crystals

Ranko M. Vrcelj,* Hugh G. Gallagher, and Peter J. Halfpenny

Read Online

ACCESS | Metrics & More | Article Recommendations | Supporting Information

ABSTRACT: Studies on the physicomechanical properties of commonly used energetic materials (EMs) that were pursued by the group led by Professor John Sherwood are reviewed in this paper. The studies ranged from the growth of high quality single crystals and the characterization of their defect and dislocation structures, mechanical testing, through to the study of polymorphism of EM crystals and fundamental aspects of crystallization processes in general. The work performed led to the definition of good growth conditions for all the EMs studied and to the full characterization of the defect structure, slip systems, and hardness properties of cyclotrimethylene trinitramine (RDX) and pentaerythritol tetranitrate (PETN). Partial characterization of the defect structures and hardness properties of cyclotetramethylene tetranitramine (HMX) and 2,4,6-trinitrotoluene (TNT) was also achieved. Additionally, fundamental crystal growth and polymorph information were defined, allowing a deeper understanding of the crystallization and crystal structure of TNT. In addition to the general review, some thoughts were given as to possible future routes for further study that could suitably utilize the complementary nature of established and modern techniques.
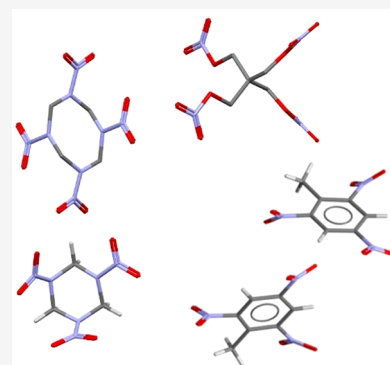
INTRODUCTION

During his career, Professor John Sherwood was instrumental in developing a deeper understanding of the crystal growth and properties of Energetic Materials (EMs). The studies were inspired and developed from earlier breakthrough work in the field, such as those by Walter McCrone, and these results still permeate ongoing studies.

John Sherwood's track record of growing large single crystals of organic materials and the analysis of their defect structure[1] led to an invitation in the late 1970s to participate in a broader study of the crystal growth, defect structures, and physicomechanical properties of some of the commonly used EMs, which ultimately continued for 20 years. Working alongside John Sherwood was Kevin Roberts with a number of students and postdoctoral staff, primarily Peter Halfpenny, Hugh Gallagher, and Ranko Vrcelj. While the direct work was focused at Strathclyde University, it led to strong working relationships and competition with both the UK (e.g., with John Field at Cambridge University) and internationally (e.g., with Ron Armstrong, then at The University of Maryland and Naval Surface Warfare Centre).

This work was originally driven by a need to understand the detonation behavior of these types of materials, particularly in relation to accidental initiation via impact. For any EM, it is desirable that they function at the appropriate time and place under appropriate stimulation. However, historical mishaps led to a realization that a better understanding of initiation was required and led to the following studies.

EMs are characterized by a number of "hazard sensitivity" tests, as defined by the North Atlantic Treaty Organisation (NATO).[2] However, for small-scale initial handling of these materials, the most important tests are chemical compatibility, electrostatic discharge, friction sensitivity, and impact sensitivity. The tests are historic, designed empirically, and satisfied the requirements of EM usage and are still in use.

These studies were part of an attempt to better understand impact sensitivity. The standard concept of initiation for EMs is that within a crystal, any energy from a stimulus can cause adiabatic heating of trapped air bubbles (or solvent) by rapid compression, leading to a "hot-spot", which will initiate the thermal process leading to initiation. At that time, it was thought that the movement of dislocations in EM crystals could "pile up" at these defect sites (e.g., air bubbles, impurity sites, inclusions, etc.), leading to unintentional "hot-spot" formation during accidental insult and lead to an unintended initiation.[3] To investigate this, an understanding of the structure and related defect structure of the EMs was required.

The studies at Strathclyde University ranged across the size scales, initially of large single crystals, but latterly of powders and additionally encompassed early computational chemistry. What connected all these studies is that they strove to understand the physical properties of the materials, using information collected at the microscopic scale and applying it to the final macroscopic state.

The published work concentrated on four commonly used EMs, cyclotrimethylene trinitramine (RDX), pentaerythritol tetranitrate (PETN), cyclotetramethylene tetranitramine (HMX) and 2,4,6-trinitrotoluene (TNT), which were, and to some degree still are, the most commonly used EMs. In real usage, these EMs are combined with at least a polymeric binder or often with another EM; however, the fundamental properties of all of them were required.

Of these materials, three of them (RDX, PETN, and HMX) decompose dangerously and violently when near or at their melting points; thus neither melt nor vapor growth methods can be used with any of these, so solution-based growth methods were utilized for all these materials.

While EMs are usually thought of in a military context, it is often overlooked that they and closely related materials are extremely common in day-to-day civilian usage, e.g., blasting, mining, demolition, etc. So, any work in these fields already has an impact on the safer and better use of such materials.

■ MATERIALS AND CRYSTAL GROWTH METHODS

All of the materials were obtained from the Propellants, Explosives and Rocket Motor Establishment (PERME), Waltham Abbey and subsequently purified. General descriptions are given in the Supporting Information (SI). More detailed descriptions are given in the cited references.

The molecular structures of each material are given in Figure 1, and the crystallographic data for each material grown as large single crystals are given in Table 1.
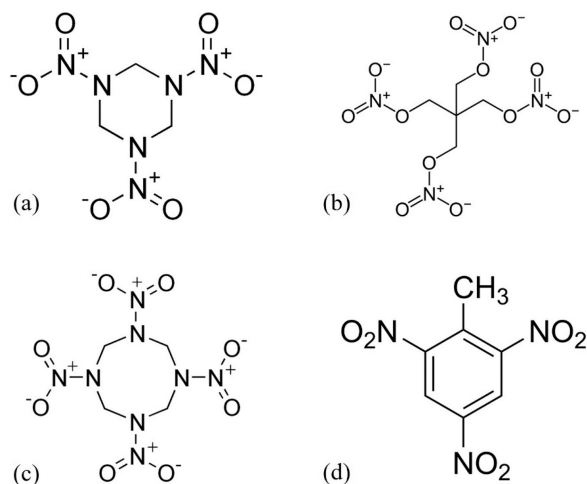

Figure 1. Molecular structures of (a) RDX, (b) PETN, (c) HMX, and (d) TNT.

For the growth of large single crystals from Seeded Controlled Cooling, the method of Sherwood et al.[8] was used across a range of temperatures and solubility ratios. A brief overview of the growth conditions is given in Table 2.

Analysis of the large single crystals was performed by a combination of X-ray topography (both laboratory and synchrotron sources), etching of surfaces, optical microscopy and both Vickers and Knoop microindentation. General experimental details are given in SI, and more detailed descriptions are given in the cited references.

RDX.[9−13] RDX is predominantly used within the military sphere as part of an explosive item and also as part of a propellant system. At room temperatures and pressures, the most stable and commonly occurring polymorph α was used in these studies (Figure 2, Table 1). RDX is polymorphic, and at room temperatures, the β form is very occasionally found (e.g., as a minor constituent in as-supplied RDX) and its structure confirmed relatively recently.[14] High temperature/pressure studies also show that further γ and ε structures are available, with the ε phase being recoverable to ambient conditions.[15,16]

Preparatory crystallization and seed production showed that solvent evaporation methods generate large seeds with well-defined morphologies, but in three different habits: equant, tabular, and prismatic.

Using controlled cooling, crystals were obtained of good optical quality, with sizes ranging ~700−3400 mm^3 (Table S1, SI) and having only prismatic habits, most likely reflecting the better control of growth conditions with this method. For these prismatic crystals, the major faces were the {210} and {111}, with smaller {110} and {010} faces, which became absent with slower growth, leading to a crystal dominated by the {210} and {111}, as shown in Figure 3.

RDX grown by this method exhibited three main types of defects, growth sector boundaries, solvent inclusions, and dislocations. Growth sector boundaries at best displayed weak changes in contrast in X-ray topographs and often none at all, showing that the lattice strain associated with these internal defects is small, although their existence could be inferred by changes of direction of some dislocations. Inclusions were rarely found. Both of these indicate good control of the growth of these crystals. Typical topographic images are given in Figure 4.

Dislocations were found at densities of 10−10^3 lines cm^{-2}, and X-ray topographic images exhibited extinction contrast ($g.b = 0$) under different diffraction conditions, leading to a classical identification of the dislocations from the extinction conditions, and a summary of these is given in SI Table S2.

All dislocations were of either a mixed or pure edge character, and in general, dislocations were generally not straight and exhibited movement even within any one growth sector.

Six distinct types of dislocation were identified in RDX and each required a separate consideration.

Type A dislocations, which propagate in the large {210} growth sectors, are straight and lie parallel to the growth normal of {210}, with Burgers vector [001]. These dislocations are of pure edge nature and are growth induced.

Type B dislocations have the Burgers vector [001] and are found in the {111} growth sectors. These follow irregular lines, in particular, helical, but generally running parallel with each other and from the crystal center to face. These are also growth induced and have undergone motion after growth.

Dislocations of type C exhibit a different character. These have Burgers vector [100] and lie in the {210} growth sectors with a mixed nature. These dislocations displayed suitably large changes form linearity, but due to their origin at, for example, solvent inclusion sites and their close propagation to the growth normal of (210) are most likely growth induced and then undergo some post growth motion.

The last major group of dislocation, type D, have Burgers vector ⟨110⟩ and lie in the {210} growth sectors, with a mixed character. Their origins were uncertain but are likely to be growth induced, with motion occurring through either glide or climb.

Less commonly appearing dislocations, types E and F, were found to likely have Burgers vector ⟨011⟩ and [010], appearing in the {210} and {111} growth sectors, respectively. Both appear to be of mixed character, but with a few examples this was not conclusive. However, this classification is likely and, if correct, suggested growth induced dislocations, with motion occurring due to either pure glide or climb.

Vickers microhardness indentation studies on RDX were also made as functions of load and temperature on the {210} faces. Cracking occurred parallel and perpendicular to [001] in all indentations, but no slip lines were observed. The Vickers Hardness number (VHN) lay in the range of 38−39 kg mm^{-2} and did not change with load. However,

Table 1. Summary of the Crystallographic Data for the EMs Grown As Large Single Crystals[a]

Material	RDX[4]	PETN[5]	HMX[6]	TNT[7]
Polymorph	α	i	β	monoclinic
a_0 (Å)	13.182	9.38	6.526	21.275
b_0 (Å)	11.574	9.38	11.037	6.093
c_0 (Å)	10.709	6.71	7.364	15.025
α (deg)	90	90	90	90
β (deg)	90	90	102.67	110.23
γ (deg)	90	90	90	90
Z, Z'	8, 1	2, 0.25	2, 0.5	8, 2
Volume (Å³)	1633.86	590.38	517.45	1828.86
Crystal system	Orthorhombic	Tetragonal	Monoclinic	Monoclinic
Space group	$Pbca$	$P\bar{4}2_1c$	$P2_1/n$	$P2_1/c$

[a]All are the most stable polymorph. Where required, descriptions of other polymorphs are given in the individual materials text sections.

Table 2. Summary of Single Crystal Growth Conditions[a]

Material	RDX	PETN	HMX	TNT
Formula	$C_3H_6N_6O_6$	$C_5H_8N_4O_{12}$	$C_4H_8N_8O_8$	$C_7H_5N_3O_6$
Solvent(s)	Acetone	Acetone	Acetone	Ethyl Acetate
		Ethyl Acetate		
Solubility (g) in 100 g solvent	12.0	24.8	2	60
		10.6		
Growth method*	C	C	C, E	C, E
Cooling range (K)	317−298	323−298	333−298	309−303
Solubility Ratio (K^{-1})	0.025	0.03	0.026	0.03
		0.03		
Mount[§]	G, N	G, N	G	G
Indentation tests	V, K	V, K	V, K	V, K

[a]*C, seeded controlled cooling; E, Solvent evaporation; [§]G is a glass rod; N, Nylon thread; [¶]V, Vickers indenter; K, Knoop indenter.
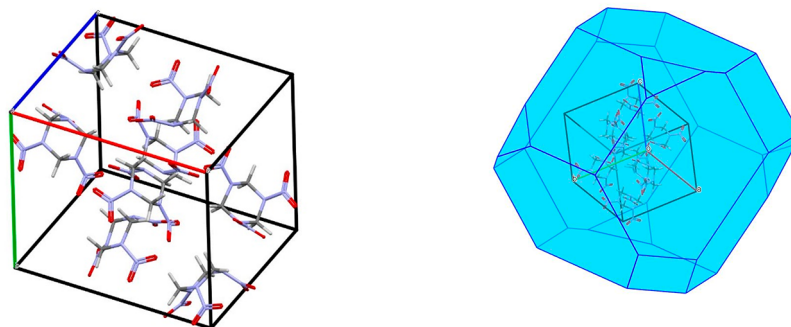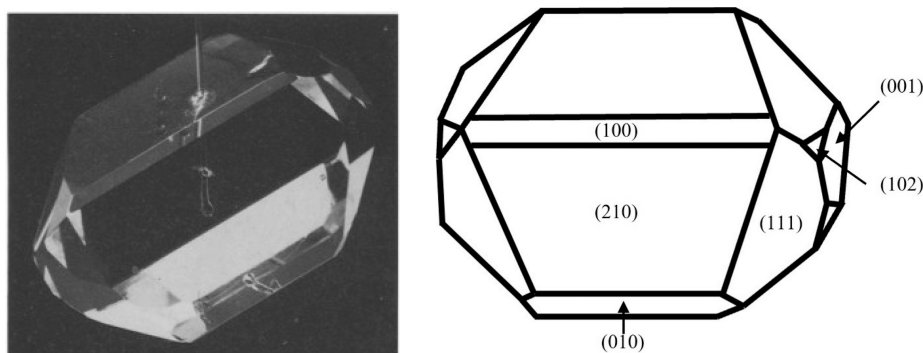

Figure 2. Crystal structure and calculated Bravais-Friedel-Donnay-Harker (BFDH) morphology of α-RDX.

Figure 3. (a) Good quality crystal of RDX. (b) Morphology.[9] Reprinted from *J. Cryst. Growth*, **1984**, 69, Halfpenny, P.J.; Roberts, K.J.; Sherwood, J.N. Dislocations in energetic materials. IV. The crystal growth and perfection of cyclotrimethylene trinitramine (RDX), 73−81, Copyright (1984), with permission from Elsevier.
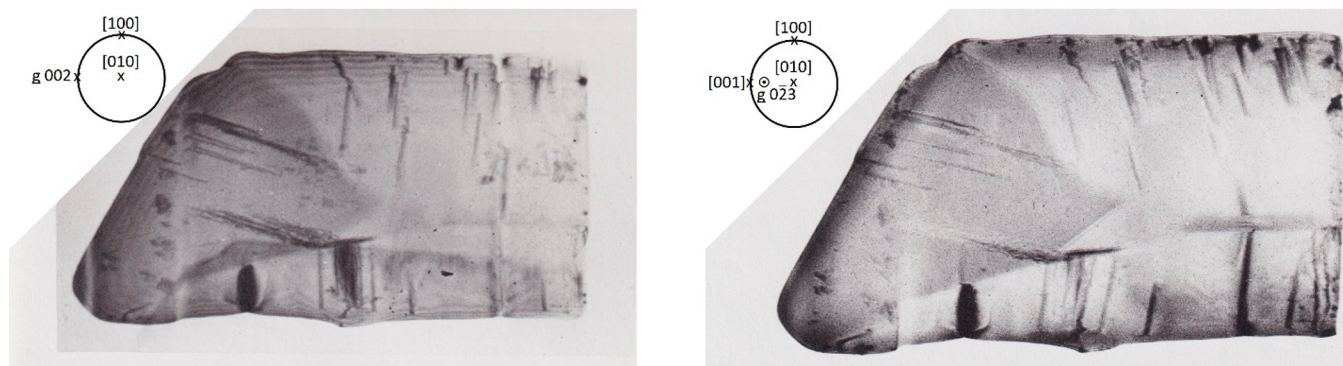
Figure 4. X-ray topographs of an RDX crystal: (a) (002) reflection; (b) (0$\bar{2}$3) reflection.
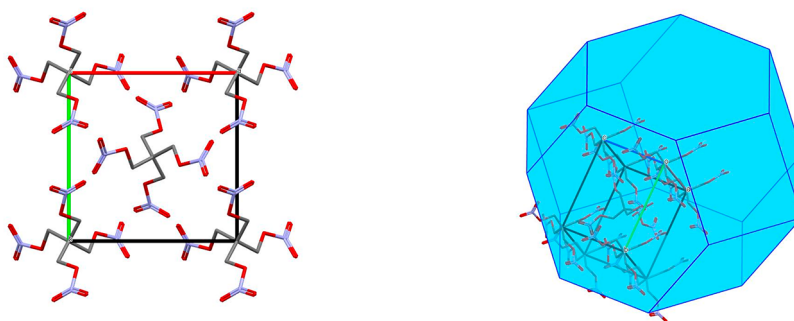

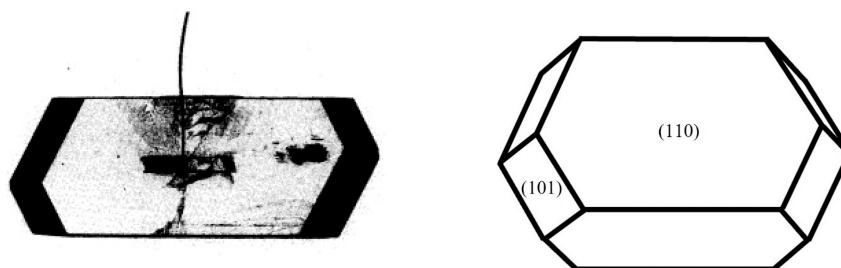**Figure 5.** Crystal structure and calculated BFDH morphology of PETN, polymorph i.

Figure 6. Left: Good quality crystal of PETN; Right: Morphology.[18] Reprinted from *J. Cryst. Growth*, **1984**, *67*, Halfpenny, P. J.; Roberts, K. J.; Sherwood, J. N. Dislocations in energetic materials. I. the crystal growth and perfection of pentaerythritol tetranitrate (PETN), 202−212, Copyright (1984), with permission from Elsevier.
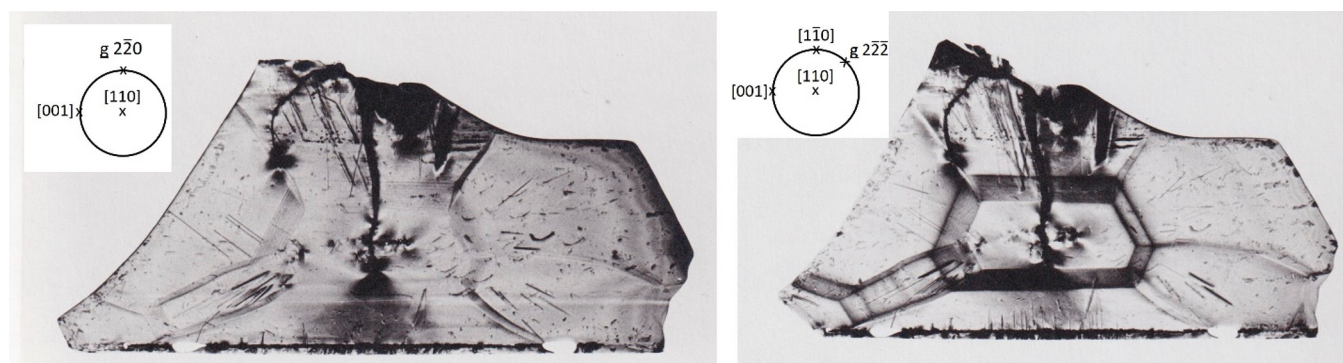

Figure 7. X-ray topographs of PETN. The individual reflections are (a) (2$\bar{2}$0); (b) (2$\bar{2}\bar{2}$).[19] Reproduced with permission of the International Union of Crystallography. Copyright 1984.

between 373 and 294 K, the hardness changed smoothly from 27 to 39 kg mm^{-2}, implying that no major changes in deformation mechanism occur.

Knoop hardness tests showed a larger variation of hardness with orientation, with the Knoop Hardness Number (KHN) ranging 32−44 kg mm^{-2}, with the lower values occurring at 0°/90°/180° from [001] and the maxima occurring at 40° and 140° from [001].

Subsequent etching and topographic imaging studies of both Vickers and Knoop indented crystals showed that from a combination of etch
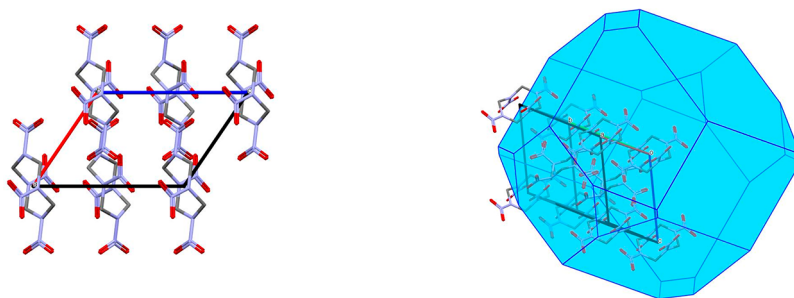
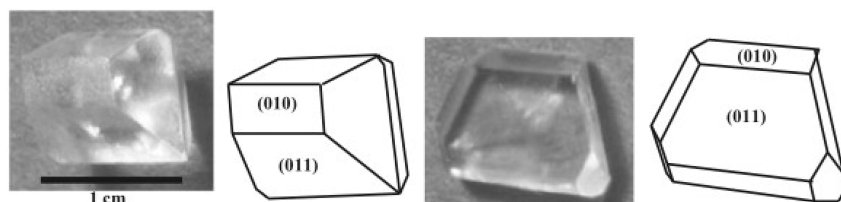**Figure 8.** Crystal structure and the calculated BFDH morphology of β-HMX.

Figure 9. Prismatic and tabular crystals of HMX with associated morphologies.[25] Reprinted from *J. Cryst. Growth*, **2017**, *475*, Gallagher, H. G.; Sherwood, J. N.; Vrcelj, R. M. The growth and perfection of β-cyclotetramethylene-tetranitramine (HMX) studied by laboratory and synchrotron X-ray topography, 192−201, Copyright (2017), with permission from Elsevier.

pit alignments and slip observations there are two major slip systems in RDX, {010}[001] and {210}[100].

This identification of the two slip systems tallies well with the calculated effective resolved shear stress (ERSS) model of Daniels and Dunn,[17] and other possible slip systems do not exhibit the same variation in ERSS as the identified systems.

PETN.[9,10,13,18,19] PETN is a secondary explosive used as a component in both the military and civilian sectors. PETN has a tetragonal structure (Table 2, Figure 5) and shows evidence of a second polymorph.[20] The following work is based on the known stable polymorph.

For PETN, solvent evaporation growth methods generate large seeds with well-defined morphologies and tabular, acicular, and prismatic habits. The single crystals grown by controlled cooling had good optical quality and generally developed a prismatic habit, with well-defined {110} and {101} forms, with smaller {111} faces and ranged in size between ∼100 mm³ and ∼4600 mm³ (SI Table S3); a typical example is shown in Figure 6.

The defects found using X-ray topography consisted of growth banding, growth sector boundaries, solvent inclusions, and dislocations. PETN seemed to more readily form solvent inclusions compared to RDX. The growth sector boundaries also exhibited a greater contrast than that of RDX, indicating a higher lattice strain associated with those features. Additionally, the contrast of the growth banding features, again indicating higher lattice strain in those areas, indicates that the crystal growth conditions were not as well controlled for PETN compared to RDX, or a greater disparity in the growth rates of the bounding faces, given that PETN grew in a less equant habit than RDX did. Typical topographic images of PETN are given in Figure 7.

Dislocation densities were on the order of $10-10^3$ lines cm⁻². Of the two growth sectors, {110} contained the most dislocations, either self-generated or dislocations refracted from {101} into {110} and the majority of dislocations apparently being of mixed edge and screw character. The underlying dislocation distribution within PETN shows no direct evidence for growth-induced dislocation motion by either glide or climb mechanisms.

In trying to definitively assess the nature of the dislocations within PETN, one fundamental issue arose, in that the typical extinction criteria for dislocation analysis often did not occur. A number of possible reasons for the lack of dislocation extinction exist: the extinction criteria apply strictly only to elastically isotropic media; mixed dislocations seldom become completely invisible; solvent or impurity decoration; weak, inaccessible, or systematically absent

reflections; superimposition of defects.[21] Given the greater number of inclusions in PETN compared to RDX, it was initially surmised that solvent decoration was the most likely cause.

However, the combination of the good image information and use of Klapper's theory of preferred dislocation line directions[22] allowed a way forward to comprehensively analyze the growth-induced dislocation structure in PETN and a summary of the results are given in SI Table S4.

Eight distinct types of dislocation could be identified throughout the crystal samples, which could be considered in three broad groups: (I) those that could be identified by experimental extinction contrast methods; (II) those that used both experimental contrast and line direction calculations; (III) those that could only be defined through line direction calculation and exhibited no experimental extinction contrast variation.

Group I consisted of the following dislocations: pure edge dislocations, with Burgers vector [001] in the $(\bar{1}10)$ growth sector, mixed dislocations with Burgers vector [001] in the $(\bar{1}0\bar{1})$ growth sector, and another mixed dislocation with Burgers vector [101] in the $(0\bar{1}1)$ growth sector.

Group II consisted of mixed dislocations, with Burgers vector [100] in the $(\bar{1}10)$ sector, and mixed dislocations of Burgers vector $[\bar{1}11]$ in the $(\bar{1}01)$ sector, but with refraction into the $(\bar{1}10)$ growth sector (and thus counted as two types).

Group III contains dislocations that were identified as mixed, the first having Burgers vector [100] in the $(10\bar{1})$ sector and the second Burgers vector [110] in the (011) growth sector.

Vickers microhardness indentation studies of PETN were performed on both {110} and {101} faces. Changes in orientation showed the characteristics of localized plastic deformation around the indentation mark and cracking, and both slip and crack directions were independent of the orientation of the indenter. The VHN of PETN barely varied with load or indenter orientation, being between 15 and 17 kg mm⁻². On increasing temperature, the hardness had a slightly wider range of values, 13−17 kg mm⁻², between 353 and 293 K, which is simply ascribed to changes in the intermolecular forces with increasing temperature.

In Knoop indentation studies of the (110) face show that the range of KHN is 13−24 kg mm⁻², with the hardest direction is parallel to $[\bar{1}10]$ and the soft directions lie at ±15° to [001].

In attempting to understand the active slip system, initial work indicated that in PETN, this was {110}[001]. However, using the ERSS

calculations, it can be seen that the best fitting slip system for PETN is, in fact $\{110\}[1\bar{1}1]$.

HMX.[23−25] HMX is a secondary explosive, predominantly used as a military explosive (Figure 8). At room temperatures, HMX exhibits polymorphism, with the most stable phase being β (Figure 6, Table 1) and less stable α, δ, and ε phases also possible.[26−28] In the work of the Sherwood group, crystals of the monoclinic β form were used.

Large single crystals of HMX were grown by both solvent evaporation and controlled cooling from acetone and had an optical quality that ranged from high to good. All solution growth methods gave crystals that exhibited four main faces, $\{010\}$, $\{101\}$, $\{011\}$, and $\{110\}$. Distinct differences in habit were observed for crystals grown via solvent evaporation, ranging from columnar, elongated along $[100]$, to tabular, with dominant $\{011\}$ faces, through to rarely observed prismatic crystals, showing only $\{010\}$, $\{011\}$, and $\{110\}$ faces. Growth under controlled temperature lowering conditions all resulted in crystals with this prismatic habit; typical examples of prismatic and tabular crystals are given in Figure 9.

The major obvious difference between HMX and the previously described PETN and RDX is the poorer quality of the crystals grown by seeded controlled cooling. Large crystals could be grown of good optical quality but only from uncontrolled solvent evaporation. Normally, growth by controlled cooling of a seed gives a crystal that is better than that of the original seed. However, in the case of HMX, the mechanical damage induced during seed preparation (attachment to a glass rod with glue, drilling, and attachment by nylon thread) caused defects, whose effects then radiate out into the future growth facets. This damage can be seen by the eye, emanating from the area surrounding the rod or thread used to mount the crystal. The crystals grown had sizes ranging ∼75−1600 mm³; the details are given in SI Table S5.

These crystals exhibited a range of defects: growth sector boundaries, dislocations, and twinning. However, solvent inclusions were not commonly seen, fewer than for either PETN or RDX, which given the increased damage of HMX under seed processing is an interesting observation, indicating that the growth conditions themselves were good enough (i.e., less chance to form large macrosteps that trap inclusions). Nevertheless, growth sector boundaries were readily observable, indicating that although the growth conditions were good, there was a higher internal strain in HMX, compared to RDX. In HMX, dislocations were found at densities of up to ∼10^8 lines cm^{-2}, and the twin plane was identified as a (101) reflection plane, confirming previous observations. A typical topographic image is shown in Figure 10.
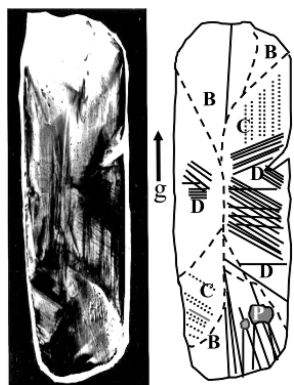

Figure 10. Left: $(02\bar{2})$ topograph of a $(01\bar{1})$ slice of a tabular crystal. Right: Schematic showing the complex nature of the growth sectors and their defect content.[25] Reprinted from *J. Cryst. Growth*, **2017**, *475*, Gallagher, H. G.; Sherwood, J. N.; Vrcelj, R. M. The growth and perfection of β-cyclotetramethylene-tetranitramine (HMX) studied by laboratory and synchrotron X-ray topography, 192−201, Copyright (2017), with permission from Elsevier.

These high dislocation densities are associated with spontaneously nucleated seeds; again given the damage associated with controlled cooling, these values will be higher for crystals grown by that method. This high number of defects means that unlike RDX and PETN, X-ray topographic imaging was always going to yield more equivocal results for HMX. Additionally, the structure and readily available morphologies of HMX meant that strong (hkl) reflections are less accessible for laboratory-based Lang Topographic methods, with only the $(02\bar{2})$ reflection being readily accessible. Synchrotron Laue methods were attempted and yielded some results; however, radiation damage, within 15 min of exposure, induced a buildup of strain in the crystals leading to "blurring out" of any contrast before adequate images could be obtained. Thus, it was not possible to perform a classical dislocation analysis via extinction contrast or to confirm identification using Klapper's method. This means that the best descriptions of the defect structure have had to be qualitative rather than quantitative.

Nevertheless, etching and associated microscopy/interferometry studies revealed some underlying information with regard to dislocation structure on the $\{011\}$, $\{110\}$, and twinned and untwinned (010) face. All etch pits suitably reflected the symmetry of the crystal faces, being complex in shape for those on $\{011\}$ and $\{110\}$, with dislocations at the base but emerging at an oblique angle to the surfaces. On (010) faces, the relative simplicity of the symmetry of the face led to more readily identifiable features. Etch pits on this face could be segregated into two families: Group 1, the predominant small, shallow, and light; and Group 2, the less common large, deep, and dark, but both having etch pit bases showing that the initiating dislocation emerges normal to the surface. Geometrical and energetic considerations led to the reasonable proposition that Group 1 dislocations are pure edge dislocations with Burgers vector $b = [100]$ and Group 2 dislocations are pure screw in character, with Burgers vector $b = [010]$. Additionally, the correspondence of etch pits between cleaved surfaces indicated they are not induced due to mechanical processing.

Microindentation hardness studies showed differences in VHN on each face, with the $\{110\}$ and $\{011\}$ faces having a range of VHNs of 30.5−32.5 kg mm^{-2} and for (010) VHN having a range of 35.5−37.5 kg mm^{-2}. For $\{110\}$ and $\{011\}$, this range remained independent of load and indenter orientation, and for (010), the range covers a slight increase in hardness with varying load. On (010) a gradual decrease of VHN occurred with increasing temperature, indicating that the deformation mechanism remained constant in this temperature range.

Knoop indention on (010) and $\{110\}$ faces showed a greater anisotropy, with the KHN varying from 32.0 to 49.2 kg mm^{-2}, depending upon indenter orientation and crystal face, with the $\{110\}$ face having a higher range of hardness number than the (010) face.

Indentation etching studies showed that the (001) and (101) planes are the two slip planes in HMX and the most likely Burgers vectors for dislocation glide on these planes as deduced from simple structural considerations are $[100]$ and $[10\bar{1}]$, respectively.

Comparisons of the Knoop hardness anisotropy with that predicted by ERSS calculations using the $(001)[100]$ and $(101)[10\bar{1}]$ slip systems showed reasonable agreement, but this requires further definitive confirmation, and it is yet too difficult to prove whether or not dislocation slip controls the deformation process during Knoop indentation.

The twinning behavior of HMX is also of interest. (101) is the defined twin plane, and it was known that twinning occurs when HMX is under compression. HMX also undergoes twinning when in tension in a similar manner. Under tension, primary twins are observed; the twinning behavior under tension described here is similar to that noted by Palmer et al. in compression.[29] In our study, two types of twins were observed. Primary twins of type (101) exist throughout the crystals at some level. Increasing tension causes the generation of secondary twins of the twin plane $(10\bar{1})$ to occur. Mechanical cycling shows that these twins appear and can grow. Reduction of tension eliminates the smaller twins, but the larger twins do not completely disappear and persist as part of the remaining crystal structure.

These studies give some excellent evidence as to why HMX is considered brittle compared to other organic solids, and the dislocation
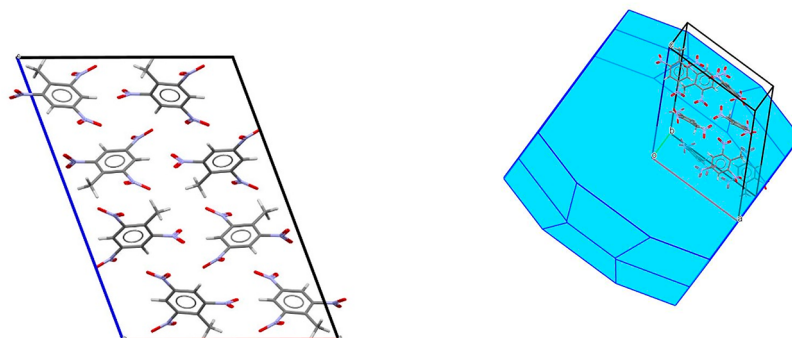
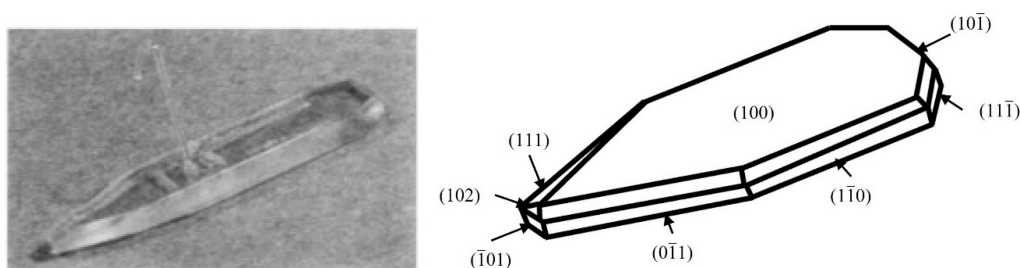**Figure 11.** Crystal structure and calculated BFDH morphology of monoclinic TNT.

Figure 12. Left: Good quality crystal of TNT; Right: Morphology.[31] Reprinted in part and adapted with permission from Gallagher, H. G.; Sherwood, J. N. Polymorphism, twinning, and morphology of crystals of 2,4,6-trinitrotoluene grown from solution. *J. Chem. Soc., Faraday Trans.*, **1996**, 92, 2107−2116. Copyright 1996. Royal Society of Chemistry.
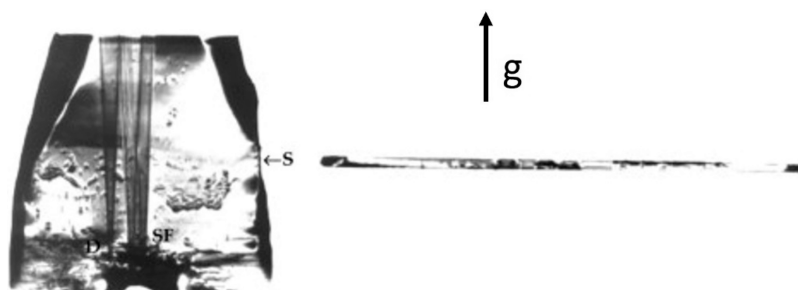

Figure 13. Left: (20$\bar{4}$) topograph of TNT displaying dislocations (D), stacking faults (SF), (S) indicates where the section topograph was taken. Right: (20$\bar{4}$) section topograph taken at position (S).[34] Reprinted from *J. Cryst. Growth* **2003**, 250. Gallagher, H. G.; Vrcelj, R. M.; Sherwood, J. N. The crystal growth and perfection of 2,4,6-trinitrotoluene, 486−498, Copyright (2003), with permission from Elsevier.

structure on the major face of β-HMX gives basic evidence as to its low plasticity.

TNT.[30−36] TNT is a secondary explosive, which although viewed as an old material and due for replacement is still used as a military explosive in a variety of compositions. At room temperatures, TNT does exhibit polymorphism, with two defined forms, the stable monoclinic (Figure 11, Table 1) and metastable orthorhombic. Unlike the previous three materials studied, TNT melts readily and is used as part of the melt cast compositions.

In addition to the single crystal studies on TNT, extensive further work was performed utilizing Single Crystal structure determination, Energy Dispersive Powder Diffraction studies, and early computational analysis.

From controlled cooling, large crystals of good optical quality were grown and exhibited only minor variations in morphology. All of the crystals were elongated in the [001] direction, and the dominant {100} form gave them a platelike habit, but {100}, {102}, {001}, {10$\bar{1}$}, {110}, {011}, {1$\bar{1}\bar{1}$}, and {111} faces were evident, although in a few crystals, the generally small {111} and {011} faces were absent. The sizes ranged ~200−4500 mm^3 (SI Table S6) and a typical example is given in Figure 12.

Single crystals grown by this method exhibited a wide range of defects, growth sector boundaries, growth banding, solvent inclusions, dislocations, stacking faults, and twinning.

TNT is notoriously hard to purify, and many of the defects are likely to be initiated by residual impurities, for example, the ready development of solvent inclusions, especially around the initial seed crystal. This also means that there is a great deal of internal lattice strain, which, although useful for generating contrast in X-ray topographs, also means that much information can be lost, as the lattice strain overwhelms more subtle changes. Typical topographic images are given in Figure 13.

In single crystal studies, the growth sectors were readily identified and growth banding evident. Again, this can be associated with the impurity driven lattice strain rather than with poor growth conditions. Some sectors appear of lighter contrast, where dislocations are evident; however, although TNT offers a good range of geometrical options for acquiring a range of topographs, no extinction contrast analysis could be performed on any individual dislocation system, apart from a single dislocation that has pure screw character and of Burgers vector b = [001]. The twinning plane was defined to be twinned by rotation of 180° about the normal to the (100) plane. Stacking faults are parallel to (100) and have a mismatch vector direction of 1/2[001].

Microindentation hardness testing on {001} faces found VHN to be 22.5 kg mm^{-2} at 295 K, independent of the orientation of the indenter and the perfection of the crystal, whereas the KHN varied with indenter orientation in the range 20.5−24.0 kg mm^{-2} at that ambient temperature. The hard and soft directions were found to lie along the [010] and [100] crystallographic directions, respectively, and KHN was found to be independent of load within the range 15−50 g.

The Knoop hardness anisotropy curve retained the same shape at 323 K indicating that there was no change in deformation mechanism up to this temperature, but the KHN values slightly decreased, which can be attributed to the change in intermolecular bonding due to thermal expansion of the lattice.

The dominant operative slip system was estimated to be {001}[010] by comparison of the Knoop hardness curve with a theoretical model based on resolved shear stress, but further confirmation of this is required.

The observations from the above studies led to modeling of the morphology of monoclinic, twinned monoclinic, and orthorhombic TNT, showing that all three had similarities in morphology, but with important differences, which can be used to define the status of any individual TNT crystal.

As part of this and as an extension of many other previous observations, it was understood that the two readily available polymorphs of TNT showed inherent and deep similarities in structure, and many previous authors, including ourselves, ascribed this to the underlying twinning monoclinic TNT readily exhibits.

However, it was shown conclusively that orthorhombic TNT, although closely related structurally to monoclinic TNT, is a different and distinct polymorph. First, in situ synchrotron Energy Dispersive Powder Diffraction studies of solution crystallization via addition of antisolvent showed that TNT behaves in accordance to Ostwald's rule of stages, with the metastable orthorhombic form appearing first, followed by the appearance of the monoclinic form and the disappearance of the orthorhombic, as shown in Figure 14. The use of the antisolvent method can effectively isolate the different polymorphs, slowing down any solvent mediated phase transformation that subsequently occurs.
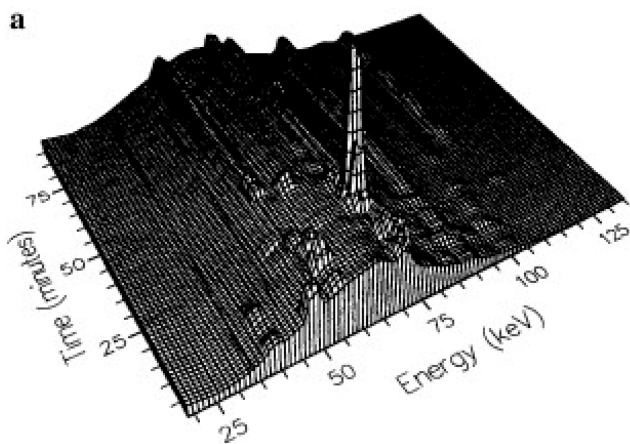

Figure 14. EDXRD traces of TNT precipitating from acetone. Reproduced from ref 33.

Alongside this, a redetermination of the crystal structures and their subsequent analysis, showed that the structures are related not by twinning, but by stacking faults. In both orthorhombic and monoclinic TNT, the molecules pack in pairs. "Properly" stacked TNT becomes monoclinic and "improperly" stacked TNT pairs generate the orthorhombic structure, as shown in Figure 15. In using the terms "properly" and "improperly", this merely refers to the energy minimal positions for stacking. Clearly, the relative ease with which orthorhombic TNT can be found means that this energy difference must be very small.
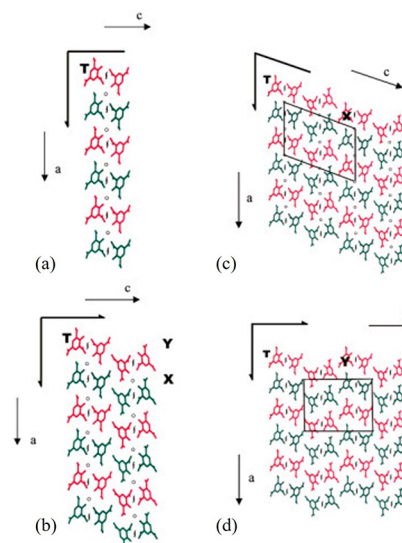

Figure 15. Building a TNT crystal, viewed parallel to the *b*-axis. (a) Stacks of pairs of TNT molecules originated at T translated along the a-glide plane. (b) Stacks of two pairs of molecules translated along the c-glide plane. (c) Placement of the next "stacks" at X to create the monoclinic form. (d) Alternative placement of the next "stacks" at Y to create the orthorhombic form. Reproduced from ref 35.

Although the differences in stacking are minimal, the resultant structures are different. Not only is the space group changed but so are the related point groups. For monoclinic, the point group is $2/m$ and for the orthorhombic is $mm2$. These then have completely different characteristics. For example, the monoclinic form has no independent third order tensor coefficients, whereas the orthorhombic form would have 5 independent third order tensor coefficients. A typical third rank tensor property is piezo-electricity.

This ability of TNT to effectively generate new polymorphs via polytypism may yet lead to the discovery of many more interesting and different structures of TNT, which themselves may have unusual physicochemical properties.

■ CONCLUSIONS

The above work was cutting edge, whether in a full dislocation analysis of RDX or PETN, assessments of their relative hardness, understanding the nature of HMX and how twinning occurs, or even the simple fundamental assessment of the structure of TNT and how that might affect its subsequent behavior.

Although the initial driver of the work, the concept of dislocation pile-up being a factor in accidental impact initiation was eventually shown to be secondary to the inclusion of grit and dirt found within EM powder samples,[37] the information gained on defect structure and distribution initiated much further thought and work on the plasticity and mechanical properties of EMs.

In the case of mechanical properties of the materials, it is clear that for both Vickers and Knoop Hardness of the studied faces, the ranking of these materials is PETN < TNT < HMX ≈ RDX.

For these materials, the full hardness testing and dislocation analyses were the first such detailed observations of these properties.

This detailed analysis led to the understanding of why PETN behaves in a more isotropic manner compared to RDX. Similar arguments can be made for HMX and TNT, although in these latter cases, the dislocation evidence is still ambiguous and requires further definition.

The analyses of these materials were based on the previous observations on less complex (ionic) structures, e.g., MgO, and while much can be derived from the simplistic models used for these, in the case of any organic material, these are further complicated by the different regime of interatomic bonding available to organic systems and the issues of steric hindrance due to the molecular conformations.

For less topologically complex systems, the active slip systems tend to be low energy, minimizing the Burgers vector associated with the system. However, the ready identification of high energy slip systems for, in particular, RDX and PETN, shows that the molecular conformation of the molecules themselves plays more of a role in the plasticity of the system. This is accentuated by the low number, low mobility, and anisotropy of the associated dislocations and contributes to, in general, the brittle nature of these materials when undergoing stress. The one exception to this is TNT, which as has been discussed above, does show direct plasticity but also is a much more complex material to understand from a mechanical perspective.

The work on EMs that John Sherwood inspired and drove not only led to a deeper understanding of the above areas but has also been the springboard from which research has developed in many associated areas, particularly with the subsequent appearance of techniques such as Atomic Force Microscopy (AFM),[38] High Temperature/Pressure diffraction methods,[39] and the development of high performance computational systems,[40,41] which at least can now be verified against experiment. A list of continuing work is as follows, although the list is not exhaustive.

1. Ongoing studies of the polymorphic nature of EMs. As with the pharmaceutical world, it is now well established that this can play role in downstream processing and final materials performance. For example, dinitroanisole (DNAN), seen as a possible replacement for TNT applications, also has polymorphism issues[42,43] of a similar vein and even the "awkwardness" of β RDX have implication in usage, especially if it is found in as-supplied material.

2. What is the inherent sensitivity of an EM? Although accidental initiation may not occur via impact, these materials must have some form of inherent sensitivity to insult. In the case of impact, this is being keenly studied, and recently some great strides have been made in developing a fundamental understanding of impact sensitivity and crystal structure.[44−46] Currently none of the hazard sensitivity tests require a knowledge of the crystal polymorph.

3. What about other sensitivity tests? For small scale testing, some empirical observations and thoughts can be made for both chemical compatibility and electrostatic discharge tests. But what about friction? Or at the larger scale? For example, how do the factors investigated above affect issues such as cook-off? Which is an accident scenario that is relatively likely to happen. Or what are issues of defect structure when these materials undergo more intense shocks?

4. The understanding of EMs from an engineering perspective. What are the roles of interfaces, whether external, e.g., with a binder, or internal, e.g., at a growth sector boundary? How do these behave when under stress and strain? These are all key elements that still need to be understood from a fundamental perspective. The role of interfaces is again a "hot topic" within the energetics community, with recent conferences such as Interfaces and Effects in Composite Energetic Materials 2021.

Work that had become unfashionable is now coming back into fashion. Single crystal growth studies are continuing within the UK, and recently at the First International Energetics Conference (IEC) in June 2022, Professor Yogendra Gupta called for "···more single crystals of EMs to be grown" during his plenary lecture[47] and also recently stated "···studies on single crystals are essential for gaining a fundamental understanding and for connecting with first-principles calculations. In my talk at the IEC, I showed some results to emphasize the importance of single crystal studies for shock compression and detonation studies."[48] The complementary nature of the microscopic methods (e.g., AFM) and macroscopic methods (e.g., X-ray topography) means that understanding how EMs behave can be mapped across the size scales and allow truly fundamental research to be performed.

Importantly, the work described was always collegiate and collaborative. Whether nationally or internationally, the work on EMs that was performed under John's aegis inspired the best scientific approaches, working alongside as many people as possible.

■ ASSOCIATED CONTENT

Ⓢ Supporting Information

The Supporting Information is available free of charge at https://pubs.acs.org/doi/10.1021/acs.cgd.3c00321.

General Experimental Descriptions with Summary tables (PDF)

■ AUTHOR INFORMATION

Corresponding Author

Ranko M. Vrcelj − *Centre for Defence Chemistry, Centre for Defence and Security, Cranfield University, Defence Academy of the U.K., Shrivenham, United Kingdom SN6 8LA;* ◉ orcid.org/0000-0001-6327-2300; Email: ranko.vrcelj@cranfield.ac.uk

Authors

Hugh G. Gallagher − *WESTCHEM, Department of Pure and Applied Chemistry, University of Strathclyde, Glasgow, Scotland, United Kingdom G1 1XL*

Peter J. Halfpenny − *WESTCHEM, Department of Pure and Applied Chemistry, University of Strathclyde, Glasgow, Scotland, United Kingdom G1 1XL*

Complete contact information is available at:
https://pubs.acs.org/10.1021/acs.cgd.3c00321

Author Contributions

The manuscript was written through contributions of all authors. All authors have given approval to the final version of the manuscript.

Notes

The authors declare no competing financial interest.

◼ REFERENCES

(1) Begg, I. D.; Narang, R. S.; Roberts, K. J.; Sherwood, J. N. X-ray topographic studies of the perfection of crystals of the organic metal: tetrathiofulvalene-tetracynoquinodimethan (TTF-TCNQ). *J. Cryst. Growth* **1980**, *49*, 735−738.

(2) Current NATO STANAG 4489 available from: https://www.nato.int/cps/en/natohq/publications.htm. Accessed 23/12/2022.

(3) Armstrong, R. W.; Coffey, C. S.; Elban, W. L. Adiabatic heating at a dislocation pile-up avalanche. *Acta Met.* **1982**, *30*, 2111−2116.

(4) Choi, C. S.; Prince, E. The crystal structure of cyclo-trimethylenetrinitramine. *Acta Crystallogr.* **1972**, *B28*, 2857−2862.

(5) Booth, A. D.; Llewellyn, F. J. The crystal structure of Pentaerythritol Tetranitrate. *J. Chem. Soc.* **1947**, 837−846.

(6) Choi, C. S.; Boutin, H. P. A study of the crystal structure of β-cyclotetramethylene tetranitramine by neutron diffraction. *Acta Crystallogr.* **1970**, *B26*, 1235−1240.

(7) Duke, J. R. C. *Personal communication*, 1981.

(8) Hooper, R. M.; McArdle, B. J.; Narang, R. S.; Sherwood, J. N. Crystallization from Solution at Low Temperatures. In *Crystal Growth*, 2nd ed. Pamplin, B., Ed.; Oxford: Pergamon, 1975.

(9) Halfpenny, P. J.; Roberts, K. J.; Sherwood, J. N. Dislocation configurations in single crystals of pentaerythritol tetranitrate and cyclotrimethylene trinitramine. *J. Cryst. Growth* **1983**, *65*, 524−529.

(10) Halfpenny, P. J.; Roberts, K. J.; Sherwood, J. N. Dislocations in energetic materials - Part 3 Etching and microhardness studies of pentaerythritol tetranitrate and cyclotrimethylenetrinitramine. *J. Mater. Sci.* **1984**, *19*, 1629−1637.

(11) Halfpenny, P. J.; Roberts, K. J.; Sherwood, J. N. Dislocations in energetic materials. IV. The crystal growth and perfection of cyclotrimethylene trinitramine (RDX). *J. Cryst. Growth* **1984**, *69*, 73−81.

(12) Halfpenny, P. J.; Roberts, K. J.; Sherwood, J. N. Dislocations in energetic materials Dislocation characterization and post-growth motion in single crystals of cyclotrimethylene trinitramine. *Philos. Mag. A* **1986**, *53*, 531−542.

(13) Gallagher, H. G.; Halfpenny, P. J.; Miller, J. C.; Sherwood, J. N. Dislocation slip systems in pentaerythritol tetranitrate (PETN) and cyclotrimethylene trinitramine (RDX). *Philos. Trans. R. Soc. London* **1992**, *A339*, 293−303.

(14) Millar, D. I. A.; Oswald, I. D. H.; Francis, D. J.; Marshall, W. G.; Pulham, C. R.; Cumming, A. S. The crystal structure of β-RDX—an elusive form of an explosive revealed. *Chem. Commun.* **2009**, 562−564.

(15) Davidson, A. J.; Oswald, I. D. H.; Francis, D. J.; Lennie, A. R.; Marshall, W. G.; Millar, D. I. A.; Pulham, C. R.; Warren, J. E.; Cumming, A. S. Explosives under pressure—the crystal structure of γ-RDX as determined by high-pressure X-ray and neutron diffraction. *CrystEngComm.* **2008**, *10*, 162−165.

(16) Millar, D. I. A.; Oswald, I. D. H.; Barry, C.; Francis, D. J.; Marshall, W. G.; Pulham, C. R.; Cumming, A. S. Pressure-cooking of explosives—the crystal structure of ε-RDX as determined by X-ray and neutron diffraction. *Chem. Commun.* **2010**, *46*, 5662−5664.

(17) Daniels, F. W.; Dunn, C. G. The effect of orientation on Knoop hardness of single crystals of zinc and silicon ferrite. *Trans. Am. Soc. Metals* **1949**, *41*, 419−442.

(18) Halfpenny, P. J.; Roberts, K. J.; Sherwood, J. N. Dislocations in energetic materials. I. the crystal growth and perfection of pentaerythritol tetranitrate (PETN). *J. Cryst. Growth* **1984**, *67*, 202−212.

(19) Halfpenny, P. J.; Roberts, K. J.; Sherwood, J. N. Dislocations in energetic materials 2. Characterization of the growth-induced dislocation structure of pentaerythritol tetranitrate (PETN). *J. Appl. Cryst.* **1984**, *17*, 320−327.

(20) Cady, H. H.; Larson, A. C. Pentaerythritol Tetranitrate II: Its crystal structure and transformation to PETN I; an algorithm for refinement of crystal structures with poor data. *Acta Crystallogr.* **1975**, *B31*, 1864−1869.

(21) Lang, A. R. Techniques and interpretation in X-ray topography. In *Diffraction and Imaging Techniques in Material Science Part 2*, Amelinckx, S.; Gevers, R.; Van Landuyt, J., Eds.; Amsterdam: North-Holland, 1978; pp 623−714.

(22) Klapper, H. *Habilitationsschrift*; RWTH: Aachen, 1975.

(23) Gallagher, H. G.; Sherwood, J. N.; Vrcelj, R. M. Growth and dislocation studies of ß-HMX. *Chem. Central Journal* **2014**, *8*, 75.

(24) Gallagher, H. G.; Miller, J. C.; Sheen, D. B.; Sherwood, J. N.; Vrcelj, R. M. Mechanical properties of β-HMX. *Chem. Central Journal* **2015**, *9*, 22.

(25) Gallagher, H. G.; Sherwood, J. N.; Vrcelj, R. M. The growth and perfection of β-cyclotetramethylene-tetranitramine (HMX) studied by laboratory and synchrotron X-ray topography. *J. Cryst. Growth* **2017**, *475*, 192−201.

(26) Cady, H. H.; Larson, A. C.; Cromer, D. T. The crystal structure of α-HMX and a refinement of the structure of β-HMX. *Acta Crystallogr.* **1963**, *16*, 617−623.

(27) Cobbledick, R. E.; Small, R. W. H. The crystal structure of the delta-form of 1,3,5,7-tetranitro-1,3,5,7-tetraazacyclooctane (δ-HMX). *Acta Crystallogr.* **1974**, *B30*, 1918−1922.

(28) Korsunskii, B. L.; Aldoshin, S. M.; Vozchikova, S. A.; Golovina, N. I.; Chukanov, N. V.; Shilov, G. V. A new crystalline HMX polymorph: ε-HMX. *Russ. J. Phys. Chem.* **2010**, *4*, 934−941.

(29) Palmer, S. J. P.; Field, J. E.; Huntley, J. M. Deformation, strengths and strains to failure of polymer bonded explosives. *Proc. R. Soc. London* **1993**, *A440*, 399−419.

(30) Gallagher, H. G.; Sherwood, J. N. Growth and perfection of single crystals of trinitrotoluene (TNT). *Mater. Res. Soc. Symp. Proc.* **1992**, *296*, 215−219.

(31) Gallagher, H. G.; Sherwood, J. N. Polymorphism, twinning and morphology of crystals of 2,4,6-trinitrotoluene grown from solution. *J. Chem. Soc. Faraday Trans.* **1996**, *92*, 2107−2116.

(32) Gallagher, H. G.; Roberts, K. J.; Sherwood, J. N.; Smith, L. A. A theoretical examination of the molecular packing, intermolecular bonding and crystal morphology of 2,4,6-trinitrotoluene in relation to polymorphic structural stability. *J. Mater. Chem.* **1997**, *7*, 229−235.

(33) Vrcelj, R. M.; Gallagher, H. G.; Sherwood, J. N. Polymorphism in 2,4,6-trinitrotoluene crystallized from solution. *J. Am. Chem. Soc.* **2001**, *123*, 2291−2295.

(34) Gallagher, H. G.; Vrcelj, R. M.; Sherwood, J. N. The crystal growth and perfection of 2,4,6-trinitrotoluene. *J. Cryst. Growth.* **2003**, *250*, 486−498.

(35) Vrcelj, R. M.; Sherwood, J. N.; Kennedy, A. R.; Gallagher, H. G.; Gelbrich, T. Polymorphism in 2−4-6 Trinitrotoluene. *Cryst. Growth Des.* **2003**, *3*, 1027−1032.

(36) Gallagher, H. G.; Sherwood, J. N.; Vrcelj, R. M. Microhardness Indentation Studies of 2−4-6 Trinitrotoluene. *Propell. Explos. Pyrotech.* **2021**, *46*, 1733−1739.

(37) Field, J. E. Hot spot ignition mechanisms for explosives. *Acc. Chem. Res.* **1992**, *25*, 489−496.

(38) Ramos, K. J.; Hooks, D. E.; Bahr, D. F. Direct observation of plasticity and quantitative hardness measurements in single crystal cyclotrimethylenetrinitramine by nanoindentation. *Philos. Mag.* **2009**, *89*, 2381−2402.

(39) Deschamps, J. R.; Frisch, M.; Parrish, D. Thermal Expansion of HMX. *J. Chem. Cryst.* **2011**, *41*, 966−970.

(40) Khan, M.; Picu, C. R. Dislocation energy and line tension in molecular crystal cyclotetramethylene tetranitramine (β − HMX). *J. Appl. Phys.* **2020**, *127*, 055108.

(41) Zecevic, M.; Cawkwell, M. J.; Ramos, K. J.; Luscher, D. J. Crystal plasticity including a phase-field deformation twinning model for the high-rate deformation of cyclotetramethylene tetranitramine. *J. Mech. Phys. Solids.* **2022**, *163*, 104872.

(42) Nyburg, S. C.; Faerman, C. H.; Prasad, L.; Palleros, D.; Nudelman, N. Structures of 2,4-dinitroanisole and 2,6-dinitroanisole. *Acta Crystallogr.* **1987**, *C43*, 686−689.

(43) Gang, X.; Gong, C.-R.; Chen, H.-Y. Crystal structure of 2,4-dinitroanisole, $C_7H_6N_2O_5$. *Z. Kristallogr.* **2007**, *222*, 321−322.

(44) Michalchuk, A. A. L.; Trestman, M.; Rudic, S.; Portius, P.; Fincham, P. T.; Pulham, C. R.; Morrison, C. A. Predicting the reactivity of energetic materials: An: ab initio multi-phonon approach. *J. Mater. Chem. A* **2019**, *7*, 19539−19553.

(45) Michalchuk, A. A. L.; Hemingway, J.; Morrison, C. A. Predicting the impact sensitivities of energetic materials through zone center phonon up-pumping. *J. Chem. Phys.* **2021**, *154*, 064105.

(46) Christopher, I. L.; Pulham, C. R.; Michalchuk, A. A. L.; Morrison, C. A. Is the impact sensitivity of RDX polymorph dependent? *J. Chem. Phys. (in press)* **2023**, *158*, 124115.

(47) Gupta, Y. M. Plenary lecture at 1st International Explosives Conference, London, June 22nd − 24th 2022.

(48) Gupta, Y. M. *Personal communication*, 2022.